Evaluation of Mach 5 Nozzle Wall Turbulent Transport Models

ROLAND E. LEE*
Naval Ordnance Laboratory, Silver Spring, Md.
AND
RUSSELL A. SMITH†
Catholic University of America, Washington, D.C.

The turbulent boundary-layer flow developed on a two-dimensional deLaval nozzle wall was systematically evaluated in terms of its transport properties. The turbulent shear stress, eddy viscosity, mixing length, and turbulent Prandtl number distributions were computed by the time-averaged conservation equations using measured mean-flow inputs. The measurements were obtained in the NOL Boundary-Layer Channel and contained controlled variations of heat transfer, Reynolds number, and pressure gradients. Definite trends relating upstream cooling, pressure gradient, Reynolds number, and heat transfer to the shear stress, eddy viscosity, mixing length, and Prandtl number were observed. In addition, a strong influence of the upstream history effect was observed in all the turbulence terms except the Prandtl number. This effect can be related to the removal of thermal energy upstream. Comparison of the turbulent shear stress with the laser-doppler velocimeter measurements showed disagreement between the measured and computed values in the inner portion of the boundary layer.

Nomenclature

APG = adverse pressure gradient flow
AW = adiabatic wall data, $T_w/T_{aw} = 1.0$
CO = conical equilibrium temperature probe data
c_p = specific heat at const pressure
CW = cold wall data, $T_w/T_{aw} = 0.25$
FPG = favorable pressure gradient flow
FW = fine-wire data
H = total enthalpy, Btu/lb
k_l = molecular thermal conductivity
k_m = Prandtl wall slope, $k_m = l/y$
l = mixing length, ft
MHT = moderate heat-transfer data, $T_w/T_{aw} = 0.8$
p = pressure, psia
p_o = tunnel supply pressure, psia
Pr_t = turbulent Prandtl number
q = local heat transfer rate, Btu/ft^2—sec
$\bar{Q}$ = estimated total heat removed, Btu/sec
Re = Reynolds number
T = temperature, °R
u, v = x and y component of velocity, ft/sec
x = distance from nozzle throat plane, in.
y = distance from nozzle wall, in.
ZPG = zero pressure gradient flow
β_δ^* = pressure gradient parameter, $[\delta^*/\tau_w)(dp/dx)]$
δ = boundary-layer thickness, in.
δ_i^* = incompressible boundary-layer displacement thickness, in.
ε = kinematic eddy viscosity, ft^2/sec
ε_h = kinematic eddy conductivity, ft^2/sec
ρ = density, lb/ft^3
τ = total shear stress, lb/ft^2
θ = compressible boundary-layer momentum thickness, in.
μ = molecular dynamic viscosity, lb-sec/ft^2

Superscript

$(\overline{\quad})$ = time average
$(')$ = fluctuating quantity

Subscript

aw = adiabatic wall
l = laminar
o = tunnel supply conditions
t = turbulent
w = wall

I. Introduction

BECAUSE of the highly complex nature of the turbulence mechanism, it is not likely that a purely theoretical solution of the governing equations for turbulent boundary-layer flows can be derived in the near future. These governing equations contain fluctuation terms which are not readily related to the dependent variables which appear in the equations. Thus, solutions of these equations employ some form of empiricism to circumvent the difficult areas.

The trend of recent analytical solutions of turbulent boundary-layer flows is toward numerical computation using finite-difference methods.[1-6] The advantages of these methods over the integral methods are their generality and flexibility whereby one can extend the application to new flow situations simply by applying the appropriate models of the turbulent-flux terms.

Although manipulation of the differential equations for different flow situations may be straightforward, the formulation of the turbulent flux models is highly empirical and depends upon detailed and reliable experimental data. In low-speed flows the hot-wire anemometer has provided the fluctuating velocity data needed to define the turbulent flux models.[7,8] In compressible flow the reliability of the hot-wire anemometer has been questioned[9] although its use has been reported by several investigators.[10-13] A newly developed instrument, the Laser-Doppler Velocimeter,[14] appears to be a good substitute for the hot-wire in high-speed compressible flow. However, its reliability is yet to be proven.

In the absence of established experimental methods, the distribution of turbulent flux terms for compressible flow have been calculated from experimental mean-flow data and the time-averaged conservation equations. These distributions are used to provide the turbulent flux models for numerical solutions. This method has been used for both incompressible[15,16] and compressible flows.[17-21] Applications of the method have been mostly for flat plate adiabatic wall flows. Extension of the method beyond the incompressible zero-pressure-gradient regime have been limited due to the lack of reliable and complete

Presented as Paper 74-96 at the AIAA 12th Aerospace Sciences Meeting, Washington, D.C., January 30–February 1, 1974; submitted February 27, 1974; revision received September 13, 1974. This work was supported by the Naval Air Systems Command under AIRTASK A320-32-C/WR02-302-003.

Index category: Boundary Layers and Convective Heat Transfer—Turbulent.

* Aerospace Engineer. Member AIAA.
† Associate Professor of Mechanical Engineering. Member AIAA.

data. The objective of the present investigation is to evaluate the expressions for the compressible turbulent flux models for shear flows with pressure gradient and heat transfer. The approach is to apply the inverse solution to the time-averaged conservation equations whereby the turbulent flux terms, namely the turbulent shear stress and turbulent heat transfer, are computed from the experimental velocity and temperature profile data. The Prandtl mixing length model and Boussinesq eddy-diffusivity concept are used to compute the kinematic eddy viscosity and eddy conductivity. The turbulent Prandtl number is defined by the ratio of the eddy viscosity to the eddy conductivity. Input data for the computational method was obtained on the sidewall of the supersonic nozzle of the Naval Ordnance Laboratory Boundary-Layer Channel.

The data used was complete in the sense that all terms needed for the solutions of the governing equations were provided by the velocity and temperature profile measurements and by the direct measurement of the local friction drag and heat transfer on the test surface. As a result of the large number of measurements which defined a single temperature and velocity profile, no elaborate data smoothing procedures were used. For each configuration of heat transfer and pressure gradient, the data were measured at four or five streamwise locations. The large number of axial stations provided increased accuracy in the determination of the flow-wise derivatives needed for the solution of the equations and eliminated the necessity of similarity assumptions which were used by previous investigators.

The effect of thermal history on the turbulent transport properties has been included in the evaluation. The thermal history is the result of substantial energy exchange between the nozzle wall and the fluid in the boundary layer in the upstream portion of the nozzle. The high energy exchange occurs commonly in the throat region of high Mach number supersonic and hypersonic nozzles and at the stagnation regions of high-speed flight vehicles.

II. Basic Equations

The equations for the steady flow mean properties of a thin boundary layer are[22]:

continuity:

$$\frac{\partial}{\partial x}(\bar{\rho}\bar{u}) + \frac{\partial}{\partial y}(\overline{\rho v}) = 0 \tag{1}$$

where $\overline{\rho v} = \bar{\rho}\bar{v} + \overline{\rho' v'}$

momentum:

$$\bar{\rho}\bar{u}\frac{\partial \bar{u}}{\partial x} + \overline{\rho v}\frac{\partial \bar{u}}{\partial y} = -\frac{\partial \bar{p}}{\partial x} + \frac{\partial \tau}{\partial y} \tag{2}$$

energy in terms of total enthalpy:

$$\bar{\rho}\bar{u}\frac{\partial \bar{H}}{\partial x} + \overline{\rho v}\frac{\partial \bar{H}}{\partial y} = \frac{\partial}{\partial y}(q + \bar{u}\tau) \tag{3}$$

The total enthalpy form of the energy equation was used to improve the computational accuracy in the numerical solution. The total enthalpy distribution across the boundary layer is normally a smoothly rising parameter with no inflections. This together with the absence of the pressure gradient term in this form would tend to reduce the computational scatter from experimental data scatter.

The total shear stress, τ, and total heat transfer, q, are sums of the laminar and turbulent contributions, respectively.

$$\begin{aligned} \tau &= \tau_t + \mu_l(\partial \bar{u}/\partial y) \\ q &= q_t + k_l(\partial \bar{T}/\partial y) \end{aligned} \tag{4}$$

Equations (1–3) were solved to obtain expressions for the total (laminar plus turbulent) shear stress and total heat transfer.

$$\tau = \tau_w + \int_o^y \frac{\partial \bar{p}}{\partial x}dy + \int_o^y \frac{\partial}{\partial x}[\bar{u}(\bar{\rho}\bar{u})]\,dy - \bar{u}\int_o^y \frac{\partial}{\partial x}(\bar{\rho}\bar{u})\,dy \tag{5}$$

$$q = q_w - \bar{u}\tau + c_p\left[\int_o^y \frac{\partial}{\partial x}(\bar{T}_o\bar{\rho}\bar{u})\,dy - \bar{T}_o\int_o^y \frac{\partial}{\partial x}(\bar{\rho}\bar{u})\,dy\right] \tag{6}$$

The laminar contribution was subtracted from the expressions for τ and q giving the turbulent fluxes which were used to determine the local eddy viscosity and eddy conductivity. In obtaining the eddy coefficients, the local velocity, and temperature derivatives $\partial\bar{u}/\partial y$ and $\partial\bar{T}/\partial y$ were numerically evaluated from the profile data by the use of the data from the two neighboring data points as follows:

$$\left(\frac{\partial x}{\partial y}\right)_n = \left(\frac{\Delta x}{\Delta y}\right)_n = \frac{x_{n+1} - x_{n-1}}{y_{n+1} - y_{n-1}} \tag{7}$$

Elaborate curve-fitting and smoothing of the data was avoided.

Equations (1–3) were derived from the equations of motion using statistical time averaging of fluctuating quantities and Boussinesq's eddy-diffusivity concepts,[23] together with Prandtl's mixing length theory.[24] Boussinesq introduced the turbulent exchange coefficient, ε, such that for simple incompressible mean flow

$$-\overline{u'v'} = \varepsilon(d\bar{u}/dy) \tag{8}$$

Prandtl introduced in his mixing length theory a length across which certain quantities in the turbulent flow were assumed to be preserved during the turbulent mixing process. Applying this principle to the velocity

$$|u'| \sim \Delta\bar{u} \sim l(\Delta\bar{u}/\Delta y) = l(d\bar{u}/dy) \tag{9}$$

and assuming further that

$$|v'| \sim |u'| \tag{10}$$

the turbulent shear stress can be expressed as

$$\tau_t = -\bar{\rho}\overline{u'v'} = \bar{\rho}|u'||v'| = \bar{\rho}l^2|(d\bar{u}/dy)|(d\bar{u}/dy) \tag{11}$$

The present-day turbulent flux models result from applications of Boussinesq's eddy-diffusivity and Prandtl's mixing length concept.

$$\tau_t = \bar{\rho}\varepsilon(\partial\bar{u}/\partial y) \tag{12}$$

$$q_t = -c_p\bar{\rho}\overline{v'T'} = \bar{\rho}\varepsilon_h(\partial\bar{T}/\partial y) \tag{13}$$

The local turbulent Prandtl number was computed by:

$$Pr_t = \varepsilon/\varepsilon_h \tag{14}$$

The numerical evaluation was performed on the Naval Ordnance Laboratory CDC 6400 high-speed computer.

Equations (12) and (13) have been the common equations used to define the turbulent exchange coefficients for flat plate flows, both compressible and incompressible. However, the complete analysis of the present supersonic nozzle flow needs to include consideration of fluctuations of the parameters other than velocity alone; namely, density, temperature, and pressure. Mixing lengths for each would be required and can be defined by the following:

$$\begin{aligned} |\rho'| &= l_\rho(d\bar{\rho}/dy) \\ |T'| &= l_T(d\bar{T}/dy) \\ |p'| &= l_p(d\bar{p}/dy) \end{aligned} \tag{15}$$

where l_ρ, l_T, and l_p are the corresponding mixing lengths for the density, temperature, and pressure, respectively. For computational simplicity the above three mixing lengths were all assumed to be equal where in reality they may not be equal. The present paper will not expand on the simplified one-mixing length concept but only evaluate the developed simplified equations for flat plate flow to describe nozzle wall flow where the mixing lengths may have strong interactions. Flat plate flow in the present context refers to the flow over a sharp leading-edge flat plate, i.e., ZPG flow with no history effects.

Historically, the expression for the turbulent shear stress as defined in Eq. (11) was simplified for incompressible flow from the more complete expression[22]

$$\tau_t = -\bar{\rho}\overline{u'v'} - \bar{u}\overline{\rho'v'} - \bar{v}\overline{\rho'u'} - \overline{\rho'u'v'} \tag{16}$$

By the order of magnitude argument for thin incompressible boundary-layer flows the last three terms can be eliminated to derive Eq. (11). Recent hot-wire anemometer results[25] showed the second term is retained for hypersonic flows. Comparison of the present results with laser-doppler velocimeter[26,27]

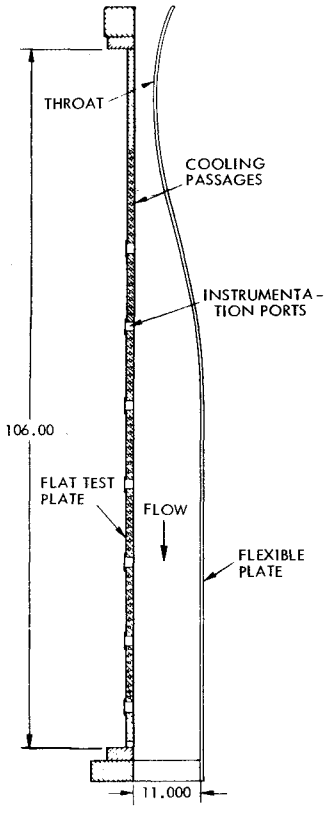

Fig. 1 Schematic of boundary-layer channel.

measurements, as will be shown, also support the retaining of the second term for supersonic flows.

III. Experimental Data

Extensive experimental mean-flow data were obtained in the Naval Ordnance Laboratory Boundary-Layer Channel facility described in Ref. 28. The facility is essentially a continuously operating blow-down wind tunnel designed specifically for boundary-layer research. The conventional symmetrical supersonic nozzle has been replaced by a nozzle having a flat test plate as one wall, a flexible plate as the other wall, and two slightly diverging sidewalls, see Fig. 1. The desired distribution of local flow properties along the test plate can be achieved by setting the flexible plate contour. Measurements taken on the flat test plate included Pitot pressure and total temperature profiles, skin friction drag, and local heat transfer rates. Detailed descriptions of the facility and its specialized boundary-layer instrumentation can be found in Refs. 28–32.

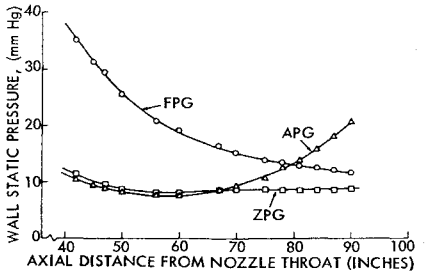

Fig. 2 Static pressure distribution along test plate.

The Mach 5 boundary-layer data used for the present evaluation were obtained for three tunnel supply pressures (1, 5, and 10 atm); three local heat-transfer rates ($T_w/T_{aw} \sim 1$, 0.8, and 0.2); and three streamwise pressure gradients (favorable, zero, and adverse). Momentum thickness Reynolds numbers ranged between 6,000 and 56,000. The streamwise pressure distributions used for the pressure gradient flow evaluation are shown in Fig. 2. For each of the above conditions, profile, shear, and heat-transfer data were measured at four or five streamwise locations. The data selected are listed in Table 1. The derivatives in the streamwise direction for the solution of Eqs. (5) and (6) were determined by a second-degree polynomial least-square fit of the measured data of all the locations.

Table 1 Data listing of run numbers

Flow condition	P_o (atm)	Measuring station (in. from nozzle throat) 50	60	70	78	84	90
ZPG-AW FW	5		001061	001073	[a]001083	001151	001121
ZPG-AW FW	1		001062	001074	[a]001084	001152	001271
ZPG-MHT FW	5		001071	001081	[a]001085	001201	001141
ZPG-MHT FW	1		001072	001082	[a]001216	001202	001261
ZPG-CW CO	10				[a]002121	002131	002161
ZPG-CW FW-CO	5		002103	012101	[a]002122	002132	002162
ZPG-CW FW-CO	1		002104	002102	[a]002123	002133	002163
APG-AW CO	10		011204	011291	[a]011201	012031	012041
APG-AW CO	5		011205	011292	[a]011202	012032	012042
APG-AW CO	1		011206	011293	[a]011203	012033	012043
APG-MHT CO	10		911111	911114	[a]911117	911121	911131
APG-MHT FW	5		911263	911264	[a]912221	912233	912241
APG-MHT FW	1		911262	911265	[a]912222	912234	912242
APG-CW CO	10		202294	202291	[a]202284	202281	202251
APG-CW CO	5		202295	202292	[a]202285	202282	202252
APG-CW CO	1		202296	202293	[a]202286	202283	202253
FPG-AW CO	10	101111	101121	[a]101131	101141	101144	
FPG-AW FW	5	101271	101275	[a]101281	101181	101285	
FPG-AW FW	1	101272	101276	[a]101282	101182	101286	
FPG-MHT CO	10	101112	101124	[a]101134		101151	
FPG-MHT FW	5	101273	101277	[a]101283	101183	101287	
FPG-MHT FW	1	101274	101278	[a]101284	101184	101288	
[b]FPG-CW CO	10		102191	203231	[a]104011	104021	
[b]FPG-CW FW	5		102192	102181	[a]102173	102171	
[b]FPG-CW FW	1		102193	102182	[a]102174	102172	

[a] Center stations where computations are made.
[b] Heat-transfer data not taken.

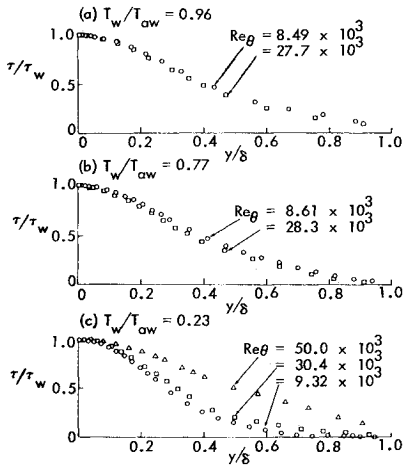

Fig. 3 Total shear stress distributions for ZPG flow, $\beta_\delta^* = 0$.

The Mach number 5 boundary-layer flow data of the NOL Boundary-Layer Channel are published in Refs. 33–38. The data selected for the present analysis are found in Refs. 36–38.

IV. Discussion of Results

The present nozzle wall boundary-layer flow is different from the conventional flat plate boundary-layer flow by the addition of two energy sources external to the shear flow. Consequently, the relatively simple turbulent diffusion process of the flat plate flow, which has been described successfully in some cases, is now influenced by the heat sink in the upstream nozzle throat region and the inviscid pressure gradient flowfield. The effects of the two energy sources on the turbulent transport terms computed from flat plate flow equations are summarized as follows:

Shear Stress Distribution

The shear stress distributions for the three heat-transfer rates at the ZPG flow are shown in Fig. 3. The distributions for FPG, ZPG, and APG flows at the adiabatic wall condition are shown in Fig. 4. For comparison the ZPG-AW values computed by the methods of Maise-McDonald[17] and Economos-Boccio[39] are plotted in Fig. 4. As predicted by the boundary-layer equations the shear stress distributions at the wall have a zero slope, negative slope, and positive slope for ZPG, FPG, and APG flows, respectively. The moderate APG flow data have a peak value less than 1.1 of the wall value and it occurs at 0.06 of the boundary-layer thickness. Similar peaks have been reported by Sturek[40] for a two-dimensional isentropic-ramp-induced APG flow at Mach 3.5. Sturek observed peak values up to 6.5 and the location of the peak to move further from the wall with increasing peak values. The distributions for all conditions showed depressions near the middle of the boundary layer. This depression, as will be described later, was due to the effect of upstream cooling.

For APG-AW flows the depressed shear stress at the mid-region of the boundary layer is approximately 60% of predicted

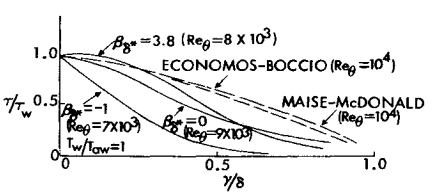

Fig. 4 Pressure gradient effect on shear stress distributions.

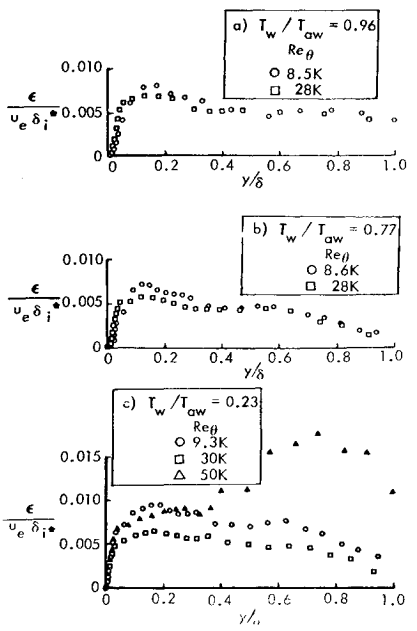

Fig. 5 Eddy viscosity distributions for ZPG flow, $\beta_\delta^* = 0$.

flat plate flow values. Similar depressions were noted by Sturek for the ZPG flow upstream of the ramp. The FPG flow shows a rapid decrease in shear stress with distance from the wall. For the FPG flow the combination of the pressure gradient and the upstream cooling effects depressed the distribution so strongly that negative shear values were produced. In the present computation the minimum value of the shear distribution was suppressed to zero to avoid the complication of negative shear stress.

Eddy Viscosity by Distribution

The kinematic eddy viscosity distributions for the three heat-transfer conditions, ZPG flow are shown in Fig. 5. The distributions for FPG, ZPG, and APG flows at the zero heat-transfer condition are shown in Fig. 6. The computed values by the methods of Maise-McDonald,[17] Economos-Boccio,[39] and Cebeci[41] are also shown in Fig. 6 for comparison. The kinematic eddy viscosity distributions show a similar depression in the mid-region of the boundary layer due to pressure gradient and upstream cooling as in the shear stress distributions. The measured values at the mid-region of the boundary are about 30% of flat plate prediction for APG-AW flows. Negative values for FPG flows were also obtained. The distribution showed an initial peaking at approximately the 15% location of the boundary layer. The magnitude of the initial peak values was correlated with momentum thickness Reynolds number and appeared to be independent of pressure gradient and local heat transfer, see Fig. 7.

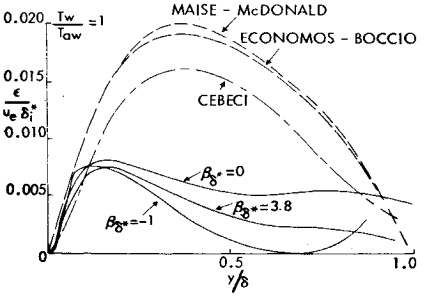

Fig. 6 Pressure gradient effect on eddy viscosity distributions.

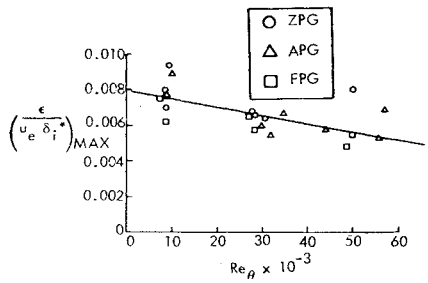

Fig. 7 Initial maximum value of $\varepsilon/u_e \delta_i^*$.

Mixing Length Distribution

The mixing length distributions for the three heat-transfer conditions, ZPG flow are shown in Fig. 8. The distributions for FPG, ZPG, and APG flows at the adiabatic wall condition and the values computed by the methods of Maise-McDonald and Economos-Boccio are shown in Fig. 9. Similar depressions of the mixing length distribution in the mid-region of the boundary layer were observed. The depression appeared either as a plateau or peak value at the 25% location and then the mixing length increased toward the outer boundary layer. The depression was about 50% of computed flat plate flow values at the mid-region for the ZPG-AW flow. Negative mixing length values also occurred for the FPG flows. The

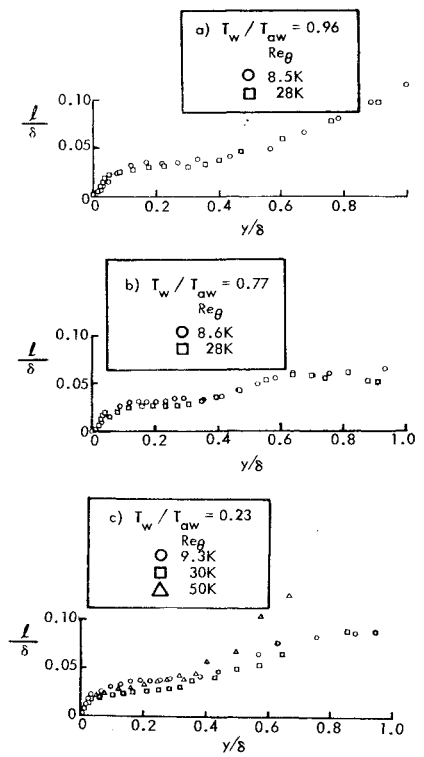

Fig. 8 Mixing length distributions ZPG flow, $\beta_\delta^* = 0$.

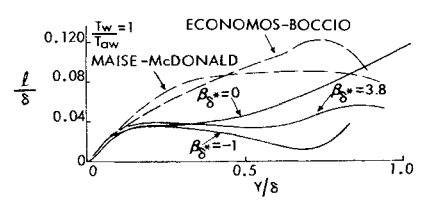

Fig. 9 Pressure gradient effect on mixing length distributions.

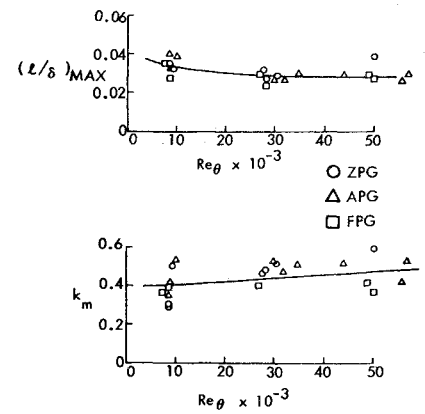

Fig. 10 Values of k_m and $(l/\delta)_{max}$.

inner 10% of the boundary layer does not appear to be altered by the pressure gradient and upstream cooling effects. Correlations of the slope of the rise, k_m, and the plateau values of the mixing length, l/δ, with momentum thickness Reynolds number are obtained, see Fig. 10. The value of k_m varied linearly with Re_θ from the value of 0.04 at $Re_\theta = 6000$, to 0.49 at $Re_\theta = 56{,}000$. The value of $(l/\delta)_{max}$ varied from 0.36 at $Re_\theta = 6000$, to an asymptotic value of 0.028 at $Re_\theta = 56{,}000$.

Turbulent Prandtl Number Distribution

The general shape of the turbulent Prandtl number distribution in the inner half of the boundary layer for the ZPG-AW flow were in good agreement with the flat plate measurements of Meier-Rotta,[19] the cone-ogive-cylinder measurements of Horstman-Owen,[20] and the prediction of Cebeci,[42] see Fig. 11. The Prandtl number is unaffected by pressure gradient or upstream cooling effects but varied systematically with Reynolds number and local heat-transfer rates, see Figs. 12 and 13. The heat-transfer effect is reflected in a lower value of Prandtl number near the wall than at the mid-region of the boundary layer. This indicates that at high heat-transfer rates the turbulent transport of heat is greater near the wall than the transport of momentum. The Prandtl number at $Re_\theta = 10{,}000$ decreases

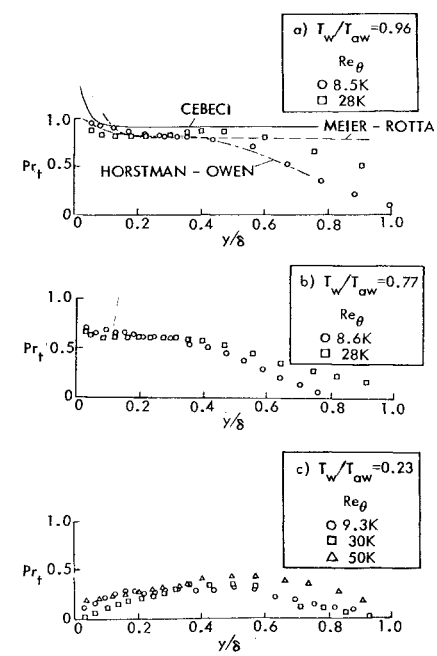

Fig. 11 Turbulent Prandtl number distributions for ZPG flow, $\beta_\delta^* = 0$.

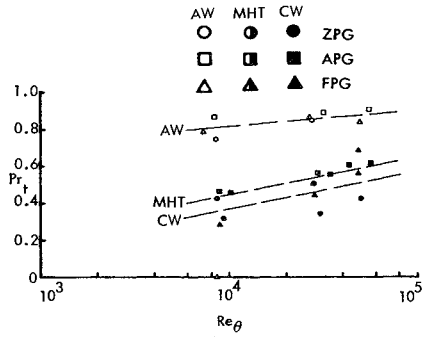

Fig. 12 Heat transfer and Reynolds number effect on the turbulent Prandtl number at $Y/\delta = 0.5$.

from the value of 0.81 for AW flow to 0.43 for CW flow at the mid-region of the boundary layer. Also at the mid-region the Prandtl number increases linearly with Reynolds number for a given heat-transfer condition. For the AW flow it increases in value from 0.8 to 0.87 for momentum thickness Reynolds numbers of 7,000 to 56,000.

Upstream Cooling

The effects of upstream cooling on the turbulent transport terms were evaluated by measuring the change in local flow properties due to the changes in the amount of cooling in the upstream nozzle throat region. A systematic test program was performed where the upstream heat removed varied from 2 to 17 Btu/sec. The effect of upstream cooling on the turbulent shear distribution and eddy viscosity is shown in Figs. 14 and 15 respectively. Systematic trends of the shear stress, eddy viscosity, and mixing length with cooling were observed, see Fig. 16 where the data were correlated at the 40% location of the boundary layer. The values of $\bar{Q}$ were computed from measured wall temperatures at the peak cooling nozzle throat region and the method of Ref. 43. No apparent effect of upstream cooling was detected in the turbulent Prandtl number distribution.

It appears from the present results that the external energy influence of the pressure gradient flowfield and the upstream cooling on the turbulent boundary layer can be compensated by the proper modifications of the turbulent transport terms computed from flat plate flow concepts.

Correlation with LDV

Although the technique for computing the turbulent transport terms from mean flow data and time-averaged equations is recognized, verification by independent means can only increase confidence in the method, particularly in the compressible flow regime. One such independent experimental method is the laser-doppler velocimeter (LDV). The LDV is an optical instrument which measures the instantaneous velocity at a point in the flow. By taking a large number of measurements and employing statistical means the velocity fluctuation terms can be extracted. Such a device has been used in the Boundary-Layer

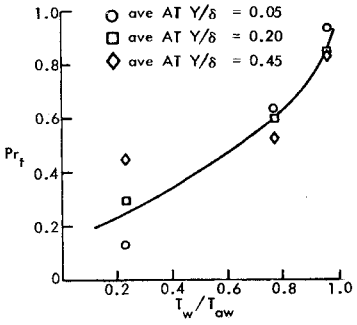

Fig. 13 Average values of Pr_t at selected Y/δ.

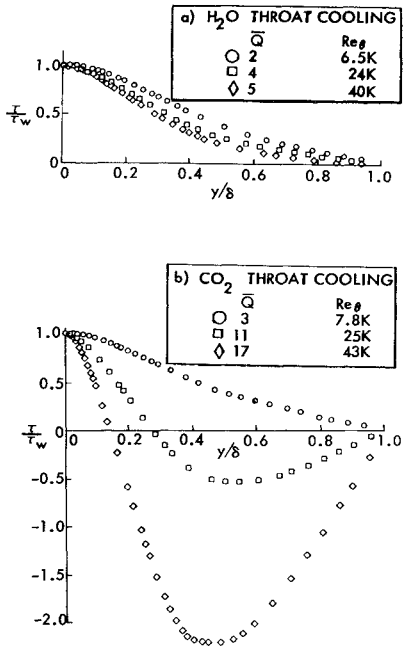

Fig. 14 Effect of upstream wall cooling on turbulent shear stress distribution, $T_w/T_{aw} = 0.96\beta_\delta^* = 1.2$.

Channel to study turbulence characteristics at Mach number three.[27] The comparison of $u'v'$ obtained by the present mean flow method and the LDV is shown in Fig. 18. The boundary-layer results agree very well at the outer portion of the boundary layer but deviate drastically at the inner portion of the boundary layer where turbulence should be more intense. The LDV results of Ref. 26 and the hot-wire measurements of Ref. 25 show the same trend as the LDV data in Fig. 18. Possible explanations for this difference are that the LDV technique has not been sufficiently refined to measure the higher turbulence intensity at the inner portion of the boundary layer, and that added higher order terms are needed to define the turbulent shear stress as shown in Eq. (16). It is apparent that more data are needed to resolve this discrepancy.

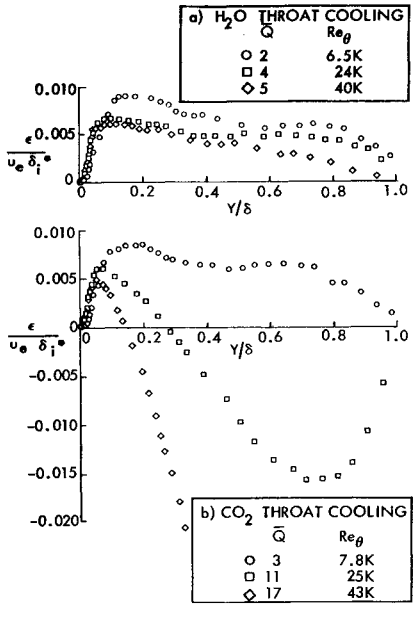

Fig. 15 Effect of upstream wall cooling on eddy viscosity distribution, $T_w/T_o = 0.96$, $\beta_\delta^* = 1.2$.

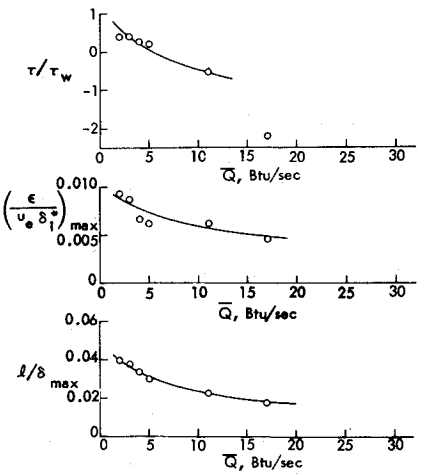

Fig. 16 Effect of $\bar{Q}$ on turbulent transport properties, $y/\delta = 0.4$.

V. Conclusion

The significant results of the present study are summarized in Table 2.

Table 2 Summary of influences on turbulent transports

Transport terms	τ	ε	l	Pr_t
Influence:				
Upstream cooling	yes	yes	yes	no
Pressure gradient	yes	no	no	no
Reynolds number	...	...	...	yes
Heat transfer	...	no	no	yes

For a given Mach number flow the controlling parameters for the development of the turbulent boundary layer on the supersonic nozzle wall were upstream cooling, pressure gradient, Reynolds number, and local heat transfer. The results showed that the upstream cooling influenced the shear stress, eddy viscosity, and mixing length distributions and not the Prandtl number distribution. Pressure gradient influenced the shear stress

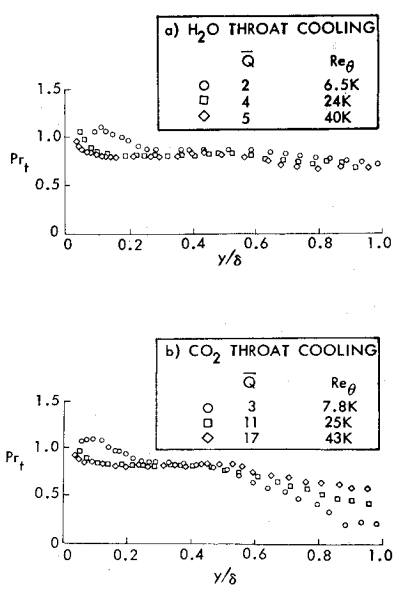

Fig. 17 Effect of upstream wall cooling on turbulent Prandtl number distribution, $T_w/T_o = 0.96$, $\beta_\delta^* = 1.2$.

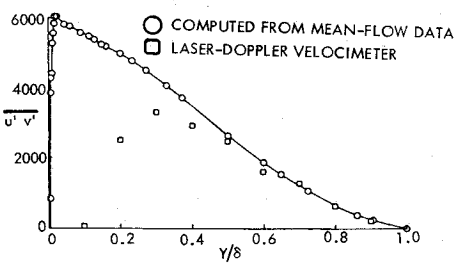

Fig. 18 Comparison between computed and measured $\overline{u'v'}$ at Mach 3, ZPG-AW.

distribution as implied by the flow equations but had no detectable effects on the eddy viscosity, mixing length, and turbulent Prandtl number distributions. The bulk of the experimental data evaluated contained a coupling of the Reynolds number influence together with the upstream cooling influence. Although correlations were made with the momentum thickness Reynolds number, uncoupling of the two influences was only possible for the turbulent Prandtl number. In that particular case, the Reynolds number has a definite influence on the turbulent Prandtl number distribution. The local heat transfer had no influence on the eddy viscosity and mixing length distributions but did affect the Prandtl number distribution. The influence of local heat transfer on the shear stress could not be determined due to overriding effects from the other influences. Systematic and significant trends were observed indicating that the influences could be quantified at least for the supersonic nozzle wall type of flows.

References

[1] Price, J. M. and Harris, J. E., "Computer Program for Solving Compressible Nonsimilar-Boundary-Layer Equations for Laminar, Transitional, or Turbulent Flows of a Perfect Gas," TM X-2458, April 1972, NASA.

[2] Herring, H. J. and Mellor, G. L., "Computer Program for Calculating Laminar and Turbulent Boundary Layer Development in Compressible Flow," CR-2068, June 1972, NASA.

[3] Patankar, S. V. and Spalding, D. B., *Heat and Mass Transfer in Boundary Layers*, Morgan-Grampian, London, 1967.

[4] Smith, A. M. O. and Cebeci, T., "Numerical Solution of the Turbulent Boundary Layer Equations," Rept. 33735, ASTIA AD656430, May 1967, Douglas Aircraft Div., the Donnell Douglas Corp., Long Beach, Calif.

[5] Cebeci, T., Mosinskis, G., and Wang, L. C., "A Finite-Difference Method for Calculating Compressible Laminar and Turbulent Boundary Layers," Rept. DAC-67131, Pts. I and II, May 1969, McDonnell Douglas Corp., St. Louis, Mo.

[6] Bushnell, D. M. and Beckwith, I. E., "Calculation of Nonequilibrium Hypersonic Turbulent Boundary Layers and Comparisons with Experimental Data," *AIAA Journal*, Vol. 8, No. 8, Aug. 1970, pp. 1462–1469.

[7] Goldberg, P., "Upstream History and Apparent Stress in Turbulent Boundary Layers," Gas Turbine Laboratory Rept. 85, May, 1966, MIT, Cambridge, Mass.

[8] Moses, H. L., "The Behavior of Turbulent Boundary Layers in Adverse Pressure Gradients," Rept. 73, Jan. 1964, Gas Turbine Lab., MIT, Cambridge, Mass.

[9] Sanborn, V. A., "Hot-Wire Anemometer Measurements in Large-Scale Boundary Layers," *Advances in Hot-Wire Anemometry* edited by W. L. Melnik and J. R. Weske, July 1968, Dept. of Aerospace Engineering, University of Maryland, College Park, Md.

[10] Kistler, A. L., "Fluctuation Measurements in a Supersonic Turbulent Boundary Layer," *The Physics of Fluids*, Vol. 2, May–June 1959, pp. 290–296.

[11] Fischer, M. C., Maddalon, D. V., Weinstein, L. M., and Wagner, R. D., "Boundary-Layer Pitot and Hot-Wire Surveys at $M = 20$," *AIAA Journal*, Vol. 9, No. 4, May 1971, pp. 826–834.

[12] Laderman, A. J. and Demetriades, A., "Measurements of the Mean and Turbulent Flow in a Cooled-Wall Boundary Layer at Mach 9.37," AIAA Paper 72-73, San Diego, Calif., 1972.

[13] Owen, F. K. and Horstman, C. C., "A Study of Turbulence

Generation in a Hypersonic Boundary Layer," AIAA Paper 72-182, San Diego, Calif., 1972.

[14] Yanta, W. J., Gates, D. F., and Brown, F. W., "The Use of a Laser Doppler Velocimeter in Supersonic Flow," AIAA Paper 71-287, Albuquerque, N.M., 1971.

[15] Squire, L. C., "Eddy Viscosity Distributions in Compressible Turbulent Boundary Layers with Injection," *The Aeronautical Quarterly*, Vol. XXII, Pt. 2, May 1971, pp. 169–182.

[16] Glowacki, W. J. and Chi, S. W., "Effect of Pressure Gradient on Mixing Length for Equilibrium Turbulent Boundary Layers," AIAA Paper 72-213, San Diego, Calif., 1972.

[17] Maise, G. and McDonald, H., "Mixing Length and Kinematic Eddy Viscosity in a Compressible Boundary Layer," *AIAA Journal*, Vol. 6, No. 1, Jan. 1968, pp. 73–80.

[18] Bushnell, D. M. and Morris, D. J., "Shear-Stress, Eddy-Viscosity, and Mixing-Length Distributions in Hypersonic Turbulent Boundary Layers," TM X-2310, Langley Research Center, Aug. 1971, NASA.

[19] Meier, H. U. and Rotta, J. C., "Temperature Distribution in Supersonic Turbulent Boundary Layers," *AIAA Journal*, Vol. 9, No. 11, Nov. 1971, pp. 2149–2156.

[20] Horstman, C. C. and Owen, F. K., "Turbulent Properties of a Compressible Boundary-Layer," *AIAA Journal*, Vol. 10, No. 11, Nov. 1972, pp. 1418–1424.

[21] Martellucci, A., Rie, H., and Sontowski, J. T., "Evaluation of Several Eddy Viscosity Models Through Comparison with Measurements in Hypersonic Flows," AIAA Paper 69-688, San Francisco, Calif., 1969.

[22] Schlichting, H., *Boundary-Layer Theory*, 6th ed., McGraw-Hill, New York, 1968.

[23] Boussinesq, T. V., "Théorie de l'écoulement tourbillant," *Mém. presentés par divers savants à l'Acad. Science*, XXIII, 46, Paris, 1877.

[24] Prandtl, L., *The Mechanics of Viscous Fluids, Aerodynamic Theory*, Vol. III, Div. G., edited by W. F. Durand, 1935.

[25] Demetriades, A. and Laderman, A. J., "Reynolds Stress Measurements in a Hypersonic Boundary Layer," *AIAA Journal*, Vol. 11, No. 11, Nov. 1973, pp. 1594–1596.

[26] Johnson, D. A. and Rose, W. C., "Measurement of Turbulence Transport Properties in a Supersonic Boundary Layer Flow Using Laser Velocimeter and Hot-Wire Anemometer Techniques," to be published in AIAA Journal.

[27] Yanta, W. J., unpublished data at Mach number 3 measured in the NOL Boundary-Layer Channel, Naval Ordnance Lab., Silver Spring, Md.

[28] Lee, R. E., Yanta, W. J., Leonas, A. C. and Carner, J. W., "The NOL Boundary-Layer Channel," NOLTR 66-185, Nov. 1966.

[29] Danberg, J. E., "The Equilibrium Temperature Probe, a Device for Measuring Temperature in a Hypersonic Boundary Layer," NOLTR 61-2, Dec. 1961, Naval Ordnance Lab., Silver Spring, Md.

[30] Yanta, W. J., "A Fine-Wire Stagnation Temperature Probe," NOLTR 70-81, June 1970, Naval Ordnance Lab., Silver Spring, Md.

[31] Bruno, J. R., Yanta, W. J., and Risher, D. B., "Balance for Measuring Skin Friction in the Presence of Heat Transfer," NOLTR 69-56, June 1969, Naval Ordnance Lab., Silver Spring, Md.

[32] Yanta, W. J. and Smith, R. A., "Measurements of Turbulent-Transport Properties with a Laser Doppler Velocimeter," AIAA Paper 73-169, Washington, D.C., Jan. 1972.

[33] Lee, R. E., Yanta, W. J. and Leonas, A. C., "Velocity profile, Skin-Friction Balance and Heat Transfer Measurements of the Turbulent Boundary Layer at Mach 5 and Zero-Pressure Gradient," NOLTR 69-106, June 1969, Naval Ordinance Lab., Silver Spring, Md.

[34] Brott, D. L., Yanta, W. J., Voisinet, R. L. and Lee, R. E., "An Experimental Investigation of the Compressible Turbulent Boundary Layer with a Favorable Pressure Gradient," NOLTR 69-143, Aug. 1969, Naval Ordinance Lab., Silver Spring, Md.

[35] Voisinet, R. L. P., Lee, R. E., and Yanta, W. J., "An Experimental Study of the Compressible Turbulent Boundary Layer with an Adverse Pressure Gradient," Paper 9, Preprint No. 93, presented at the AGARD Conference on Turbulent Shear Flows, Sept. 1971, London, U.K.

[36] Voisinet, R. L. P. and Lee, R. E., "Measurements of a Mach 4.9 Zero-Pressure-Gradient Turbulent Boundary Layer with Heat Transfer, Part I—Data Compilation," NOLTR 72-232, Sept. 27, 1972.

[37] Voisinet, R. L. P. and Lee, R. E., "Measurements of a Compressible Adverse Pressure Gradient Turbulent Boundary Layer with Heat Transfer, Part I—Data Compilation," to be published in a Naval Ordnance Laboratory Report.

[38] Voisinet, R. L. P. and Lee, R. E., "Measurements of a Supersonic Favorable-Pressure-Gradient Turbulent Boundary Layer with Heat Transfer—Pt. I: Data Compilation," NOLTR 73-224, Dec. 1973, Naval Ordnance Lab., Silver Spring, Md.

[39] Economos, C. and Boccio, J., "An Investigation of the High Speed Turbulent Boundary Layer with Heat Transfer and Arbitrary Pressure Gradient," Pts. I, II, and III, NASA CR-1679, Dec. 1970, General Applied Science Labs., Inc., Westbury, Long Island, New York.

[40] Sturek, W. B., "Turbulent Boundary-Layer Shear Stress Distributions for Compressible Adverse Pressure Gradient Flow," *AIAA Journal*, Vol. 12, No. 3, March 1974, pp. 375–376.

[41] Cebeci, T., "Calculations of Compressible Turbulent Boundary Layers with Heat and Mass Transfer," *AIAA Journal*, Vol. 9, No. 6, June, 1971, pp. 1091–1097.

[42] Cebeci, T., "A Model for Eddy-Conductivity and Turbulent Prandtl Number," Rept., MDC-J0747/01, McDonnell Douglas Corp., St. Louis, Mo., May 1970.

[43] Persh, J. and Lee, R. E., "A Method for Calculating Turbulent Boundary Layer Development in Supersonic and Hypersonic Nozzles Including the Effects of Heat Transfer," NAVORD Rept. 4200, June 1956, Naval Ordnance Lab., Silver Spring, Md.